Published in final edited form as:
J Nat Prod. 2010 March 26; 73(3): 435–440. doi:10.1021/np900645c.

4-Arylflavan-3-ols as Proanthocyanidin Models: Absolute Configuration via Density Functional Calculation of Electronic Circular Dichroism[⊥]

Yuanqing Ding[†], **Xing-Cong Li**[†,‡,*], and **Daneel Ferreira**[†,‡,*]

[†]National Center for Natural Products Research, Research Institute of Pharmaceutical Sciences, The University of Mississippi, University, Mississippi 38677

[‡]Department of Pharmacognosy, School of Pharmacy, The University of Mississippi, University, Mississippi 38677

Abstract

Density functional theory/B3LYP has been employed to optimize the conformations of selected 4-arylflavan-3-ols and their phenolic methyl ether 3-*O*-acetates. The electronic circular dichroism spectra of the major conformers have been calculated using time-dependent density functional theory to validate the empirical aromatic quadrant rule applied to the assignment of the absolute configuration of this class of compounds. The modest 6–31G* basis set was sufficient to produce reasonable spectra. The calculated Cotton effects between 220–240 nm, crucial for the assignment of the C-4 absolute configuration, results from electronic transitions of the molecular orbitals involving the π-electrons of the spatially close aromatic A-ring and 4-aryl moieties. The sign of this Cotton effect is determined by the orientation of the 4-aryl substituent: the negative and positive Cotton effects are associated with 4α-and 4β-aryl substituents, respectively.

The proanthocyanidin class of naturally occurring polyphenols has attracted considerable attention over the last several years. Their biological and industrial applications depend on an understanding of their composition, configuration, and conformational behavior including rotation about the interflavanyl bonds and preferred conformations of the heterocyclic dihydropyran rings. Owing to the structural complexities of such polymers, essential features of their dynamic behavior are reliant on projections from monomers and oligomers with limited structural variety. A range of 4-arylflavan-3-ols has thus been synthesized[1] as models for configurational and conformational studies of the naturally occurring proanthocyanidins. The conformations of the heterocyclic dihydropyran rings in these compounds were proposed based on the ^{1}H NMR coupling constants, while the assignment of the C-4 absolute configuration by experimental electronic circular dichroism (ECD) was consistent with the aromatic quadrant rule[2] and exciton coupling3 between the electronically allowed transitions of the A-and D-ring aromatic chromophores.

Recent development of density functional theory (DFT) calculations has opened a new avenue for the structural analysis of chiral molecules.[4] The calculated ECD spectrum of the compound

[⊥]Dedicated to the late Dr. John W. Daly of MDDK, NIH and to the late Dr. Richard E. Moore of the University of Hawaii at Manoa for their pioneering work on bioactive natural products.

*To whom correspondence should be addressed. Tel: 662-915-6742. Fax: 662-915-7989. xcli7@olemiss.edu (X.-C. Li). Tel: 662-915-7026. Fax: 662-915-6975. dferreir@olemiss.edu (D. Ferreira).

Supporting Information Available: Detailed computational calculating data of compounds **1a–4a** and **1b**. This information is available free from the Internet at http://pubs.acs.org.

of interest provides critical conformational and configurational information: the closer the calculated and experimental ECD spectra are, the better the calculated conformation and configuration reflects the compound behavior in solution. The purpose of this study was to employ such advanced computational methods to assess the conformations and configurations of selected 4-arylflavan-3-ols in order to understand the theoretical basis of the empirical aromatic quadrant rule applied to the assignment of the absolute configuration of this class of compounds.

Results and Discussion

Four 4-arylflavan-3-ols, (2*R*,3*S*,4*S*)-3',4',7-trihydroxy-4-(2,4,6-trihydroxyphenyl)flavan-3-ol (**1a**), (2*R*,3*S*,4*S*)-3',4',7-trihydroxy-4-(2,4-dihydroxyphenyl)flavan-3-ol (**2a**), (2*R*,3*R*,4*R*)-3',7,8-trihydroxy-4-(2,4,6-trihydroxyphenyl)flavan-3-ol (**3a**), and (2*S*,3*S*,4*R*)-3',4',7-trihydroxy-4-(2,4,6-tri-hydroxyphenyl)-flavan-3-ol (**4a**) and their corresponding phenolic methyl ether 3-*O*-acetates (**1b–4b**), were selected as models. These molecules and their enantiomers represent all possible C-ring configurational diastereoisomers of naturally occurring proanthocyanidins. This selection was also based on the availability of experimental ECD spectra of **1b–3b** and numerical experimental ECD data of **1a, 2a**, and **4b**.[1] Compounds **1a** and **1b** with a 4α-aryl group and, thus, 4*S* absolute configuration, exhibited a high-amplitude, diagnostic negative Cotton effect (CE) in the 220–240 nm region, while compounds **2a** and **2b–4b** with 4β-aryl groups (4*S* absolute configuration for **2a** and **2b**; 4*R* for **3b** and **4b**) gave positive CEs in the same region. The 4-arylflavan-3-ols (**1a** and **2a)** and their respective methyl ether 3-*O*-acetates (**1b** and **2b**), devoid of intra- and inter-molecular hydrogen bonding interactions, essentially gave experimental ECD data similar to the derivatized analogs.[1]

A systematic conformational search was carried out for compound **1b** via Monte Carlo random search in the SYBYL 8.1 program using MMFF94 molecular mechanics force-field calculation. An energy cutoff of 10 kcal/mol was used to generate a wide window of conformers in the Boltzmann population, affording 153 conformers. For the first 50 conformers, the B-ring, acetoxy group, and D-ring are equatorially positioned while C-4 is coplanar with the A-ring. Next, the 25 conformers with lowest energies were geometrically optimized using DFT at the B3LYP/6–31G* level. Four predominant conformers, **1b1–1b4**, were relocated with a Boltzmann distribution of 17.3, 44.6, 19.1, and 19.0% by Gibbs free energy (Table 1). The major differences between the four conformers are the orientation of the B-ring and *O*-methyl groups (Figure 1). Their key dihedral angles are shown in Table 2. The C2-O1-C9-C10 and C3-C4-C10-C9 dihedral angles are −20° and −14° to −16°, respectively, in **1b1–1b4**, indicating that C-2 and C-3 of the hetereocyclic dihydropyran ring are located above and below the A/C plane, respectively, permitting the B-ring and the 3-*O*-acetyl group to extend equatorially. The D-ring is located below the A/C plane of the flavan-3-ol moiety, and hence in the lower left quadrant, as evidenced by the C1″-C4-C10-C9 dihedral angle of approximately −142° in the four conformers. The H-C2-C3-H dihedral angle in **1b1–1b4** ranges from 173° to 178°, supporting a large coupling constant of 10.0 Hz between H-2 and H-3 in the experimental ^{1}H NMR spectrum, while the H-C3-C4-H dihedral angle of 166 ° to 168° is consistent with a $^{3}J_{3,4}$ value of 9.0 – 9.8 Hz.[1a–1c,1e]

TDDFT calculations of the predominant conformer **1b2** at the B3LYP/6–31G* (gas phase), B3LYP/6–311++G**//B3LYP/6–31G* (gas phase), and B3LYP-SCRF/6–31G*//B3LYP/6–31G* [COnductor-like continuum Solvent MOdel (COSMO)5] levels afforded ECD spectra shown in Figure 2 (A). The weighted ECD spectra from the four conformers (**1b1–1b4**) are shown in Figure 2 (B). The excellent match of the calculated and experimental ECD spectra for compound **1b** indicates that such computational methods are reliable for the conformational and configurational analysis of this class of compounds.

Based on the optimized conformations of **1b** and consideration of the C2″OH…OC3 hydrogen bonding, a starting geometry of compound **1a** was set up to scan its potential energy surfaces (PESs) by rotating the B and D-rings about the C-2-C-1′ and C-4-C-1″ bonds at the B3LYP/6–31G* level (gas phase) (Figure 3). Six minima (**1a1–1a6**, Figure 4) were found and relocated by further optimization at the same level and confirmed by computation of harmonic vibrational frequencies. Hydrogen bonding is present between C2″OH…OC3 in **1a1** and **1a2** and between C3OH…OC2″ in **1a3** and **1a4**. It is interesting that this PES scan and optimization also afforded conformers **1a5** and **1a6** with π-stacking interactions[1e] between the B- and D-rings, in which the C1′-C2-O1-C9 dihedral angles are 102° and 101°, respectively, while the C1″-C4-C10-C9 dihedral angles are −111° in both conformers. However, conformational analysis indicated that **1a1** and **1a2** were the predominant conformers with populations of 52 and 48%, respectively, by Gibbs free energy (see Table 3). The key dihedral angles in **1a1** and **1a2** are similar to those in **1b1** and **1b2**, respectively, except for the minor difference of the C2″-C1″-C4-C10 dihedral angle (−142° vs. −118° in **1a** and **1b**, respectively) (Table 2). The H-C2-C3-H and H-C3-C4-H dihedral angles are 179° and 161°, respectively, in both **1a1** and **1a2**, also supporting the respective $^{3}J_{2,3}$ and $^{3}J_{3,4}$ ^{1}H NMR coupling constants of 10.0 and 9.8 Hz for compound **1a**.[1a, 1c]

Similarly, TDDFT calculations of the ECD spectra of conformers **1a1** and **1a2** were conducted at the B3LYP/6–31G* level. The calculated CE around 230 nm corresponds well with the experimentally observed high-amplitude negative CE at 237 nm for compound **1a** (Figure 5).[1e] It seems that this CE results from the negative rotatary strengths at 237 (MO103→MO106), 227.3 (MO104→MO108), 226.9 (MO102→MO107), 221 (MO104→MO110), and 220 (MO100→ MO106) nm in **1a1** and those at 237 (MO103→MO106), 228 (MO104→MO108), 223 (MO100→MO106), and 220.4 (MO104 →MO110) nm in **1a2** (Table 4). However, the biggest contributions are from the electronic transition from MO104→MO108 in both **1a1** and **1a2**. The calculated molecular orbitals (MOs) of **1a1** show that MO104 and MO108 involve the π-electrons of the A-ring and 4-aryl moieties (Figure 6). This strongly indicates that the diagnostic CE of this class of compounds in the 220–240 nm region of their CD spectra derives from the chiral perturbation of the two spatially close aromatic chromophores, and provides theoretical evidence to interpret the empirical aromatic quadrant rule: the 4α-aryl substituent located in the lower left quadrant makes a negative contribution to the CE at 220–240 nm in the CD spectrum.[1e]

The effects of solvent and basis set have also been evaluated by computations at the B3LYP-SCRF/6–31G*//B3LYP/6–31G* level with the COSMO model in MeOH and at the B3LYP/6–311++G**//B3LYP/6–31G* level in the gas phase. The ECD curves for both conformers **1a1** and **1a2** and the weighted curve of compound **1a** at both the B3LYP-SCRF/6–31G*//B3LYP/6–31G* and B3LYP/6–311++G**//B3LYP/6–31G* levels were similar to those at the B3LYP/6–31G* level, though a red shift occurred for the wavelengths of identified excitations, e.g., for conformer **1a1**, the excitations at 227.3 and 226.9 nm at the B3LYP/6–31G* level in the gas phase shifted to 230 and 229 nm at the B3LYP-SCRF/6–31G*//B3LYP/6–31G* level and to 228.1 and 227.5 nm at the B3LYP/6–311++G**//B3LYP/6–31G* level, respectively.

The above results demonstrated that the calculated ECD spectra of the free phenolic 4-arylflavan-3-ol (**1a**) and its corresponding methyl ether 3-*O*-acetate (**1b**) were consistent with their experimental data. In addition, the modest B3LYP/6–31G* basis set was sufficient to produce reasonable spectra. To save computational time, we only performed ECD calculations of compounds **2a–4a** at the B3LYP/6–31G* (gas phase) and B3LYP-SCRF/6–31G*//B3LYP/6–31G* (solution) levels, which we believe would also reflect the anticipated results from the corresponding methyl ether 3-*O*-acetate (**2b–4b**).

Based on the optimized geometries of **1a**, the substituents at C-2, C-3, and C-4 were all set as equatorial, as a starting geometry to scan the PES of **2a** at the B3LYP/6–31G* level by rotating the D-ring about the C-4-C-1″ bond (Figure 7). Six conformers (**2a1–2a6**) were found and relocated by optimizations at the same level. The orientation of the B-ring and the hydrogen bonding between C2″OH…OC3 and between C3OH…OC2″ in **2a1–2a4** (Figure S1, Supporting Information) are similar to those in **1a1**–**1a4**. For **2a5** and **2a6**, C2″OH…OC3 hydrogen bonding was permitted in a conformation with a C2″-C1″-C4-C10 dihedral angle of 157° (Figure 7). The C2″-C1″-C4-C3 dihedral angles in **2a1–2a6** are 38, 43, 90, 90, −80 and −80°, respectively (Table 2). Conformational analysis indicated that conformers **2a5** and **2a6** are 40 and 60% populated, respectively, by Gibbs free energy (see Table S4, Supporting Information). The H-C2-C3-H dihedral angles in all conformers of **2a** are from 172° to 176° and those of H-C3-C4-H from 26° to 48°, supporting the experimental ^{1}H NMR data ($J_{2,3}$ 8.0, $J_{3,4}$ 5.0 Hz 1a). The C1″-C4-C10-C9 and C1″-C4-C10-C5 dihedral angles are 104° and −77°, respectively, in both **2a5** and **2a6**, indicating that the 4β-aryl substituent is located in the upper left quadrant, which would make a positive contribution to the CE in the 220–240 nm region of the ECD spectrum according to the empirical aromatic quadrant rule.[1c,2]

The calculated ECD spectra of conformers **2a5** and **2a6**, weighted ECD spectra of **2a**, and the experimental ECD spectrum of **2b** are shown in Figure 8. It shows clearly that the calculated positive CE in the 220–240 nm region (consistent with the experimentally observed positive CE at 238 nm for **2a**1e) supports the prediction by the aromatic quadrant rule.1c,2

The starting geometry of **3a** was based on the optimized geometry of **2a**. The B- and D-rings were set equatorially and the 3-hydroxy group axially. Another factor was the consideration of the intramolecular hydrogen bonding between C8OH…O1. Conformational optimizations at the B3LYP/6–31G* level indicated that a conformer (**3a1**) (Figure 9) with an intramolecular hydrogen bonding between C8OH…O1 was 99.9% populated compared to the conformer without the hydrogen bonding. Conformer **3a1** did not possess hydrogen bonding between C2″ OH…OC3 as in **1a1** and **1a2** due to the α-axial position of the 3-hydroxy group and the *trans*-orientation of the 3-hydroxy and 4-aryl substituent (D-ring). Despite the differences of the C-ring configurations, **3a1** has a C-ring conformation similar to those of **1a, 1b**, and **2a**, as indicated by the C2-O1-C9-C10 and C3-C4-C10-C9 dihedral angles (Table 2). As in **2a5** and **2a6**, the 4-aryl substituent is located in the upper left quadrant, which would lead to a positive CE in the 220–240 nm region of the ECD spectrum according to the empirical aromatic quadrant rule.[1c,2]

The calculated ECD spectrum of **3a1** and the experimental ECD spectrum of **3b** are shown in Figure 9 (assuming **3a** and **3b** having similar ECD spectra). The two experimentally observed positive CEs in the 220–240 nm region of the ECD spectrum are corroborated by the two strong positive rotatory strengths at 226 and 216 nm in the calculated ECD spectrum at the B3LYP/6–31G* level (gas phase), again supporting the applicability of the aromatic quadrant rule.[1c, 2]

For the last compound (**4a**) in our study set, the B- and D-rings were similarly equatorially oriented and the C2″OH…OC3 intramolecular hydrogen bonding was considered when setting up the starting conformation to scan the PES by rotating the C-2-C-1′ and C-4-C-1″ bonds at the B3YP/6–31G* level (Figure 10). Six conformers (**4a1–4a6**) were found and confirmed at the same level. The C2″OH… OC3 hydrogen bonding was found in **4a1, 4a2, 4a5**, and **4a6** (Figure 10) and C2″O…HOC3 hydrogen bonding in **4a3** and **4a4** (Figure S3, Supporting Information). However, conformational analysis indicated a distribution of 28, 50, 8, and 14% for the predominant conformers **4a1, 4a2, 4a5**, and **4a6**, respectively, by Gibbs free energy. These differ as far as the orientation of the 3-hydroxy group is concerned (Figure 11). A distinguishing feature for this seemingly sterically hindered molecule is the change of the C-

ring conformation, primarily due to the inversion of the C-2 configuration when compared to the aforementioned compounds. The C2-O1-C9-C10 and C3-C4-C10-C9 dihedral angles range between 13–21° and 21–22°, respectively, in the four conformers (Table 2), indicating that C2 and C3 are located below and above the A/C-plane, respectively. Although the C1″-C4-C10-C9 dihedral angles in **4a1, 4a2, 4a5**, and **4a6** increased to about 153° when compared to those of **2a5** (104°), **2a6** (104°), and **3a1** (114°), the 4-aryl substituent (D-ring) is still located in the upper left quadrant. Thus, compound **4a** would show a positive CE in the 220–240 nm region of the ECD spectrum. The experimentally observed positive CE at 236 nm in **4b** (assuming **4b** and **4a** showing similar ECD spectra) was indeed consistent with the prediction, implying that the conformational inversion of the C-ring will not change the sign of the positive CE in the 220–240 nm region. Again, the calculated ECD spectra of **4a** showing a strong positive CE in the 220–240 nm CD region (Figure 9) provided theoretical support to validate the applicability of the aromatic quadrant rule to define the absolute configuration at C-4 of 4-arylflavan-3-ols.

In summary, DFT/B3LYP has been employed to locate the conformational minima of representative 4-arylflavan-3-ols and their corresponding phenolic permethyl ether 3-*O*-acetates. TDDFT has been performed to calculate their ECD spectra to validate the empirical aromatic quadrant rule. The diagnostic CE in the 220–240 nm region of the ECD spectra of this class of compounds originates from the chiral perturbation of the spatially close aromatic A-ring and C-4 aryl moieties. The sign of this CE is determined by the orientation of the 4-aryl substituent: negative and positive CEs are associated with 4α- and 4β-oriented aryl substituents, respectively. These theoretically calculated conformational and ECD characteristics of 4-arylflavan-3-ols may be extended to also address the issue of the absolute configuration of the naturally occurring proanthocyanidins.

Experimental Section

Methods of Computational Calculations

The calculations were performed by the SYBYL 8.1 program (Tripos International, St. Louis, MO) and the Gaussian03 program package.6 MMFF94 molecular mechanics force-field and potential energy surface (PES) were employed to search the possible conformations. All ground-state geometries were optimized at the B3LYP/6–31G* level at 298 K, and harmonic frequency analysis was computed to confirm the minima. TDDFT5 at the same level was employed to calculate excitation energy (in nm) and rotatory strength R (velocity form R^{vel} and length form R^{len} in 10^{-40} erg-esu-cm/Gauss) between different states. The ECD spectra were then simulated by overlapping Gaussian functions for each transition according to

$$\Delta \in (E) = \frac{1}{2.297 \times 10^{-39}} \frac{1}{\sqrt{2\pi}\sigma} \sum_{i}^{A} \Delta E_i R_i e^{-[(E-\Delta E_i)/(2\sigma)]^2}$$

where σ is the width of the band at 1/e height and ΔE_i and R_i are the excitation energies and rotatory strengths for transition *i*, respectively. Both the R^{vel} and R^{len} forms can be used for the simulation of the ECD spectrum, while the latter may provide better results.[4a] In this work, σ = 0.10 eV and R^{vel} were used.

Supplementary Material

Refer to Web version on PubMed Central for supplementary material.

Acknowledgments

We thank the Mississippi Center for Supercomputing Research (MCSR) for computational facilities. This work was supported in part by the USDA Agricultural Research Service Specific Cooperative Agreement No. 58-6408-2-0009 and NIH AI027094.

References and Notes

1. (a) Botha JJ, Ferreira D, Roux DG. J. Chem. Soc., Chem. Commun 1978:698–700. (b) Botha JJ, Young DA, Ferreira D, Roux DG. J. Chem. Soc., Perkin Trans. I 1981:1213–1219. (c) Van der Westhuizen JH, Ferreira D, Roux DG. J. Chem. Soc., Perkin Trans. I 1981:1220–1226. (d) Steynberg JP, Burger JFW, Young DA, Brandt EV, Ferreira D. Heterocycles 1989;28:923–935. (e) Van Zyl PW, Steynberg JP, Brandt EV, Ferreira D. Magn. Reson. Chem 1993;31:1057–1063.
2. DeAngelis GG, Wildman WC. Tetrahedron 1969;25:5099–5112.
3. (a) Harada, N.; Nakanishi, K. Circular Dichroic Spectroscopy - Exciton Coupling in Organic Stereochemistry. Oxford University Press; Oxford, UK: 1983. (b) Gaffield W, Foo LY, Porter LJ. J. Chem. Res. (S) 1989:144–145.
4. (a) Diedrich C, Grimme S. J. Phys. Chem. A 107 2003:2524–2539. (b) Crawford TD, Tam MC, Abrams ML. J. Phys. Chem. A 2007;111:12058–12068. (c) Stephens PJ, Pan J-J, Devlin FJ. J. Org. Chem 2007;72:2508–2524. [PubMed: 17338574] (d) Stephens PJ, Devlin FJ, Gasparrini F, Ciogli A, Spinelli D, Cosimelli B. J. Org. Chem 2007;72:4707–4715. [PubMed: 17516678] (e) Ding Y, Li X-C, Ferreira D. J. Org. Chem 2007;72:9010–9017. [PubMed: 17958369] (f) Berova N, Bari LD, Pescitelli G. Chem. Soc. Rev 2007;36:914–931. [PubMed: 17534478] (g) Ding Y, Li X-C, Ferreira D. J. Nat. Prod 2009;72:327–335. [PubMed: 19099470]
5. (a) Klamt A, Schürmann G. J. Chem. Soc. Perkin Trans. II 1993;2:799–805. (b) Klamt A. J. Phys. Chem 1995;99:2224–2235. (c) Eckert F, Klamt A. AIChE J 2002;48:369–385.
6. Frisch, MJ.; Trucks, GW.; Schlegel, HB.; Scuseria, GE.; Robb, MA.; Cheeseman, JR.; Montgomery, JA., Jr; Vreven, T.; Kudin, KN.; Burant, JC.; Millam, JM.; Iyengar, SS.; Tomasi, J.; Barone, V.; Mennucci, B.; Cossi, M.; Scalmani, G.; Rega, N.; Petersson, GA.; Nakatsuji, H.; Hada, M.; Ehara, M.; Toyota, K.; Fukuda, R.; Hasegawa, J.; Ishida, M.; Nakajima, T.; Honda, Y.; Kitao, O.; Nakai, H.; Klene, M.; Li, X.; Knox, JE.; Hratchian, HP.; Cross, JB.; Adamo, C.; Jaramillo, J.; Gomperts, R.; Stratmann, RE.; Yazyev, O.; Austin, AJ.; Cammi, R.; Pomelli, C.; Ochterski, JW.; Ayala, PY.; Morokuma, K.; Voth, GA.; Salvador, P.; Dannenberg, JJ.; Zakrzewski, VG.; Dapprich, S.; Daniels, AD.; Strain, MC.; Farkas, O.; Malick, DK.; Rabuck, AD.; Raghavachari, K.; Foresman, JB.; Ortiz, JV.; Cui, Q.; Baboul, AG.; Clifford, S.; Cioslowski, J.; Stefanov, BB.; Liu, G.; Liashenko, A.; Piskorz, P.; Komaromi, I.; Martin, RL.; Fox, DJ.; Keith, T.; Al-Laham, MA.; Peng, CY.; Nanayakkara, A.; Challacombe, M.; Gill, PMW.; Johnson, B.; Chen, W.; Wong, MW.; Gonzalez, C.; Pople, JA. Gaussian 03, Revision B. 02. Pittsburgh PA: Gaussian, Inc.; 2003.

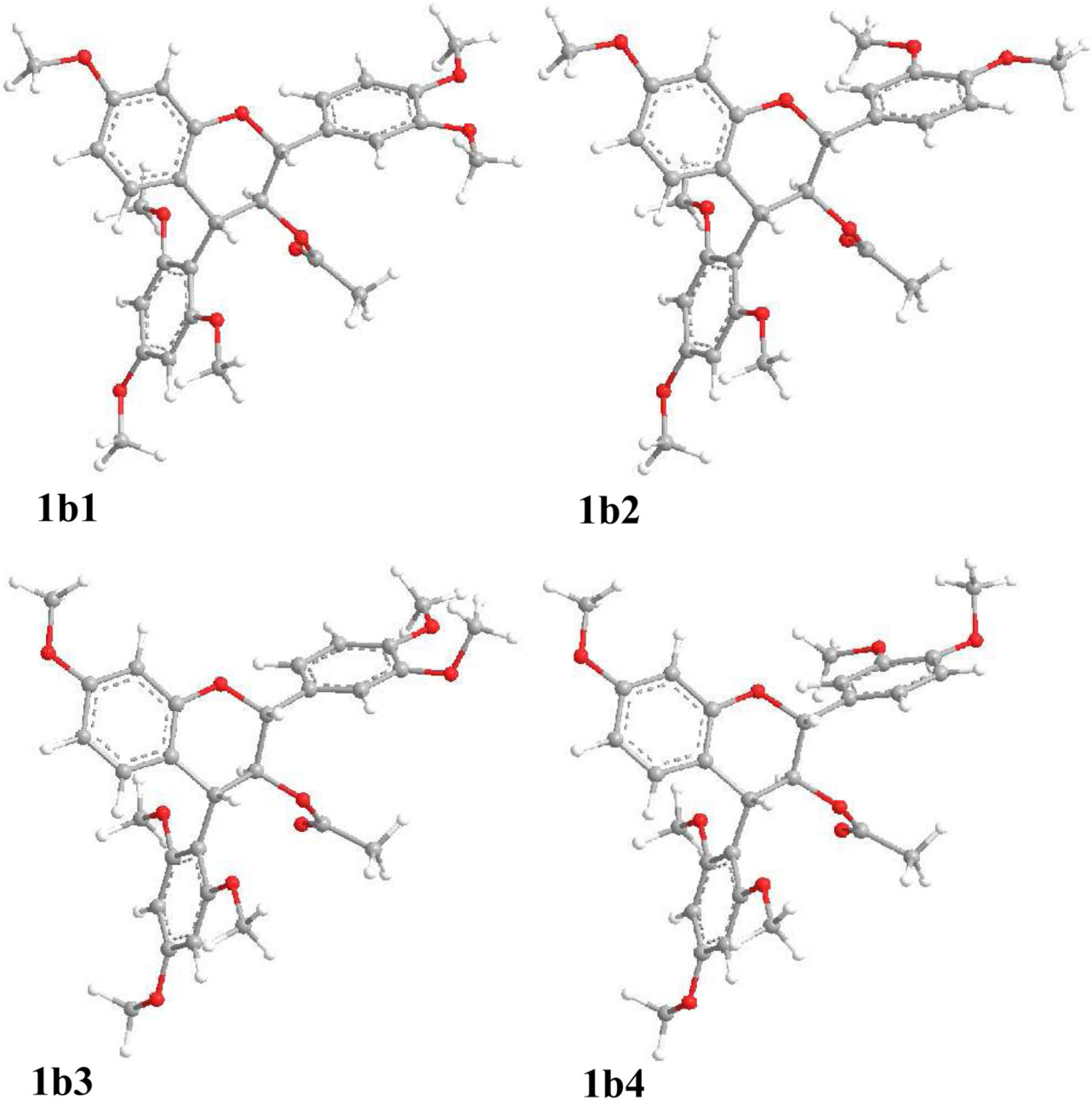

Figure 1.
Optimized geometries of predominant conformers of **1b** at the B3LYP/6–31G* level in the gas phase.

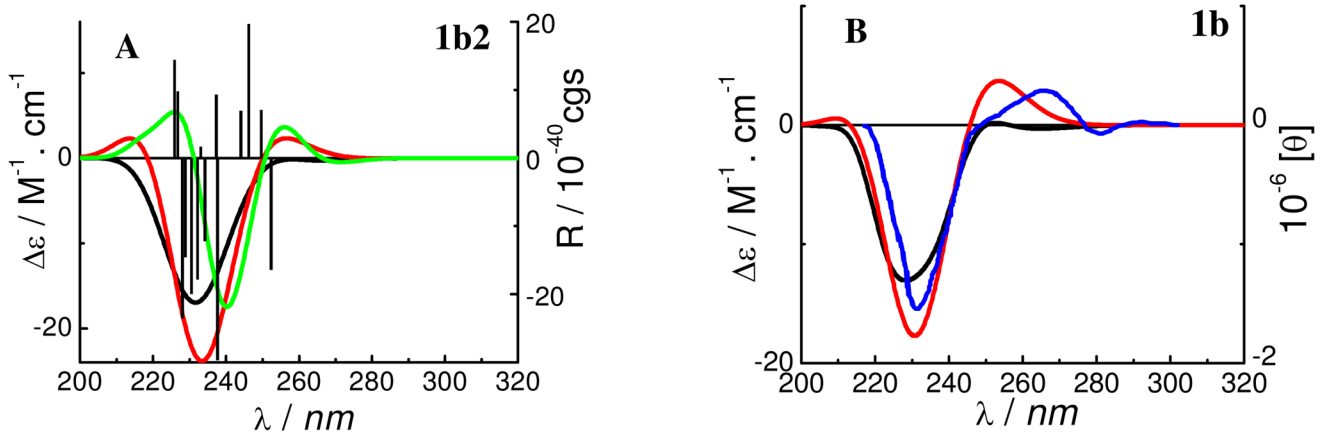

Figure 2.

Calculated ECD spectra of conformer **1b2** (A) and weighted and experimental ECD spectra of compound **1b** (B). (— and —: at the B3LYP/6–31G* and B3LYP/6–311++G**//B3LYP/6–31G* levels in the gas phase, respectively; —: at the B3LYP-SCRF/6–31G*//B3LYP/6–31G* level with the COSMO model in MeOH; —: the experimental ECD spectrum in MeOH).

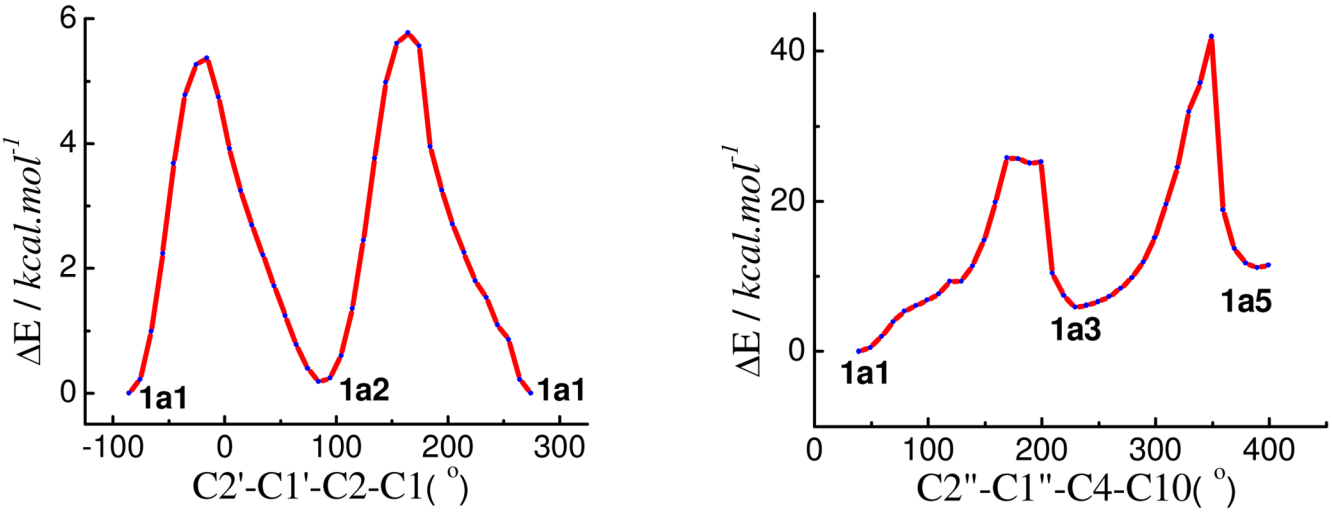

Figure 3.
Potential energy surface of compound **1a** at the B3LYP/6–31G* level in the gas phase by rotating the B-ring about the C-2-C-1′ and the D-ring about C-4-C-1″.

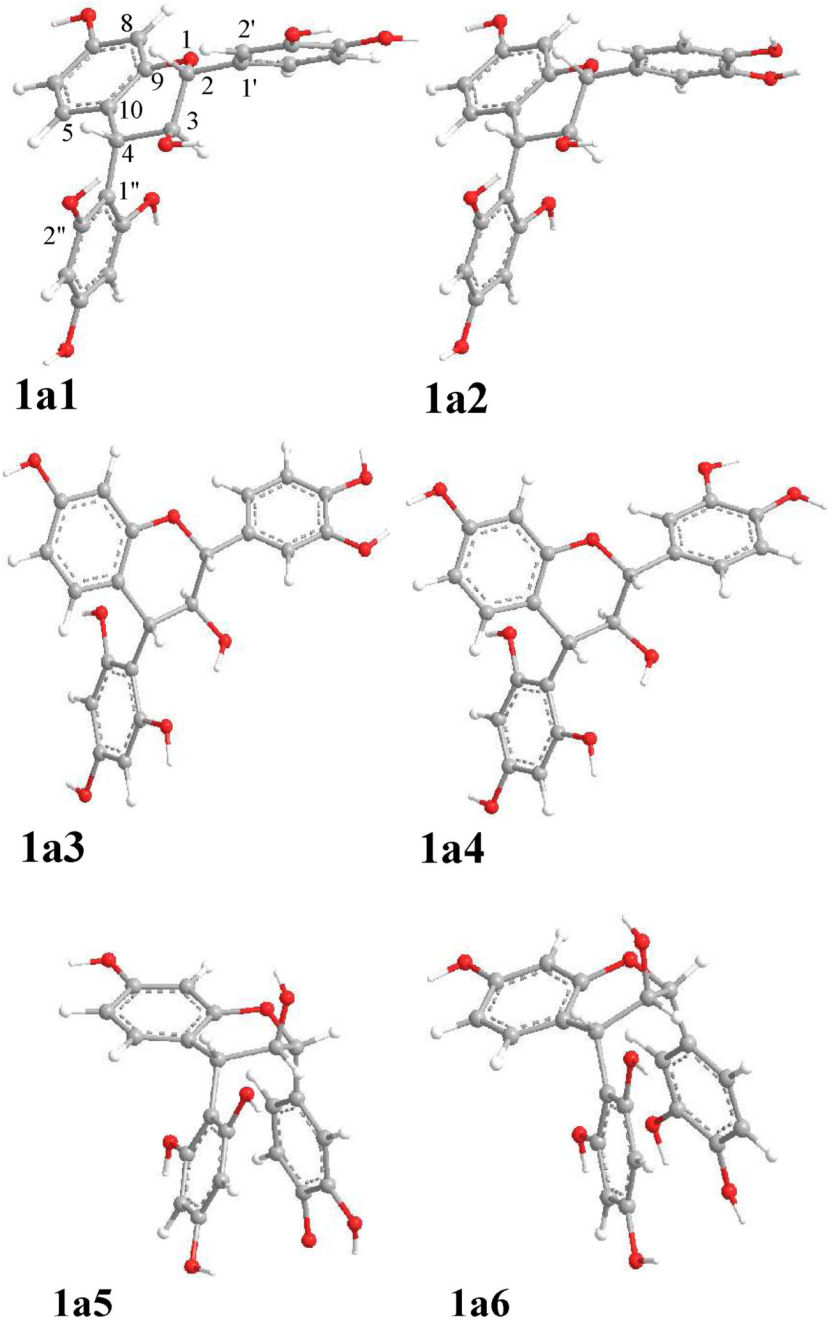

Figure 4.
Optimized geometries of conformers **1a1–1a6** at the B3LYP/6–31G* level in the gas phase.

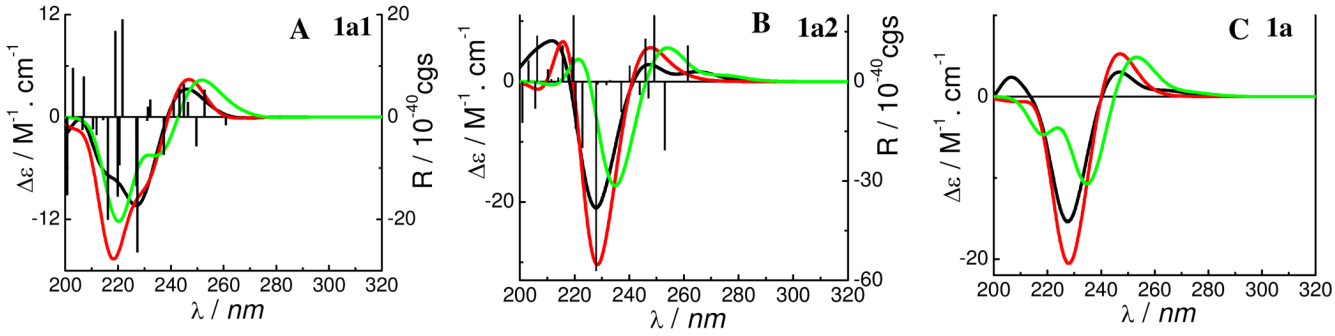

Figure 5.

Calculated ECD of predominant conformers of compound **1** (A, B) and its weighted ECD (C). (— and —: at the B3LYP/6–31G* and B3LYP/6–311++G**//B3LYP/6–31G* levels in the gas phase, respectively; —: at the B3LYP-SCRF/6–31G*//B3LYP/6–31G* level with the COSMO model in MeOH).

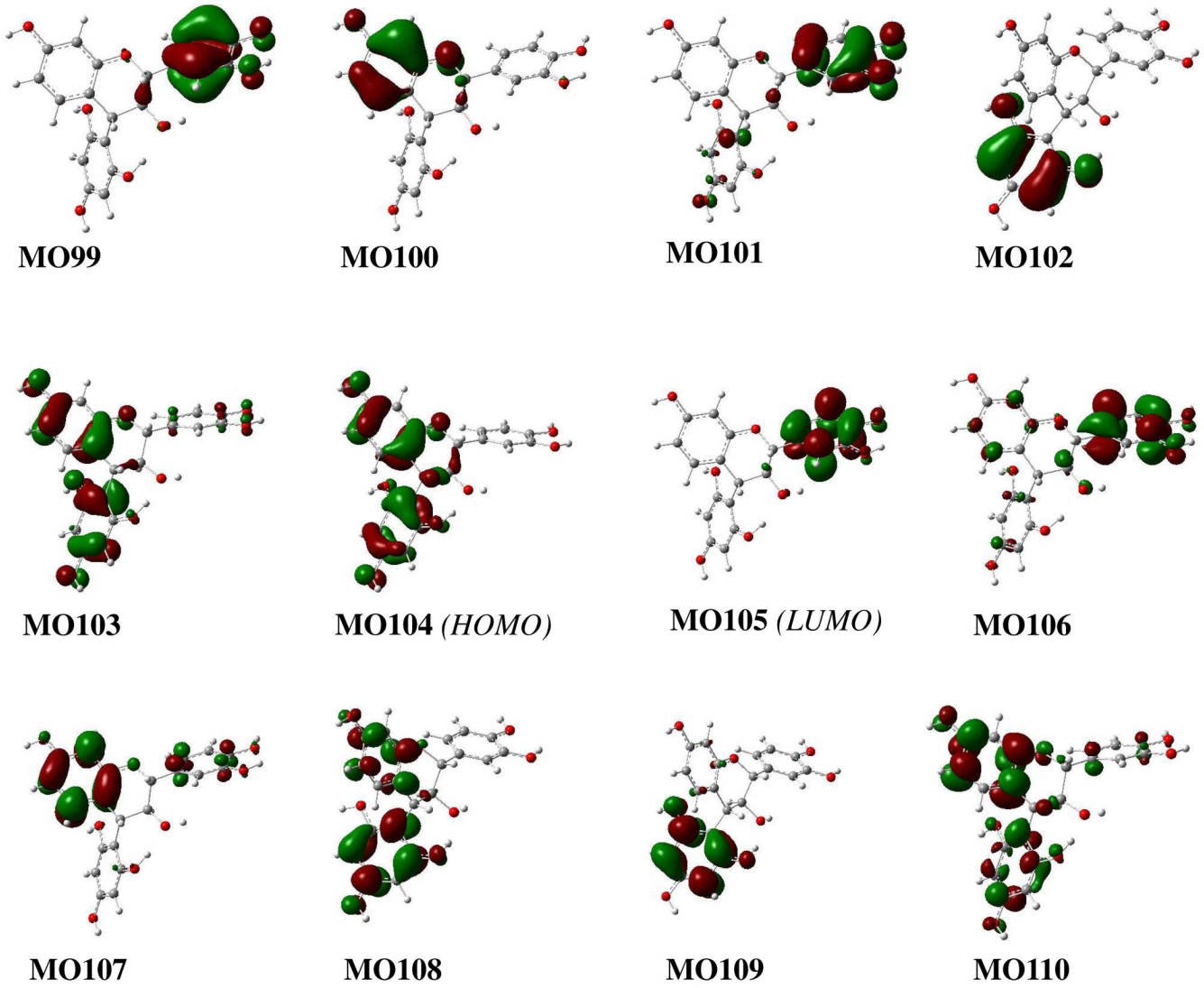

Figure 6.
Some molecular orbitals involved in important transitions regarding ECD spectra of conformer **1a1** in the gas phase at the B3LYP/6–31G* level.

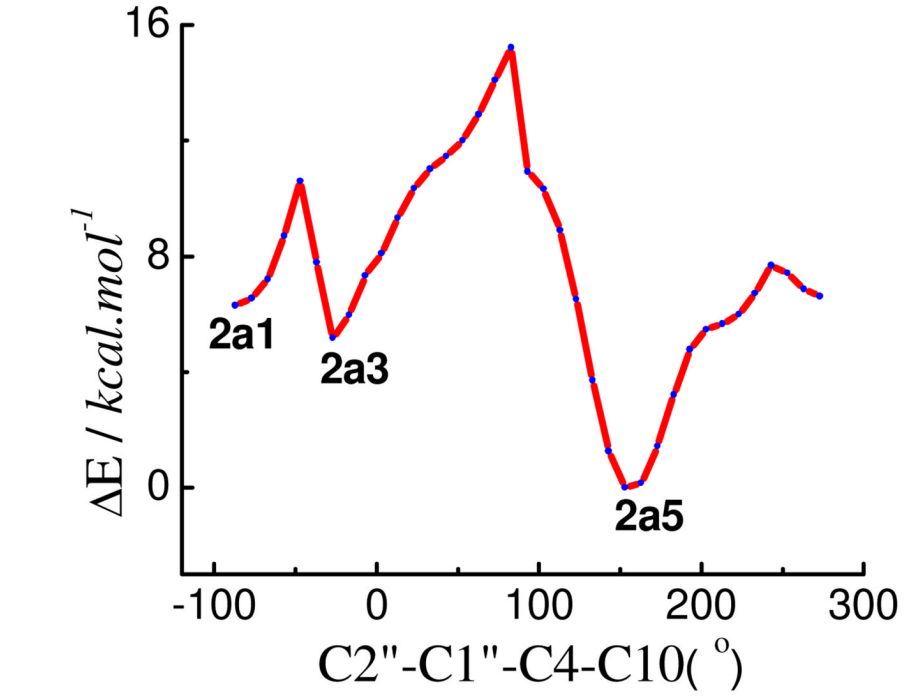

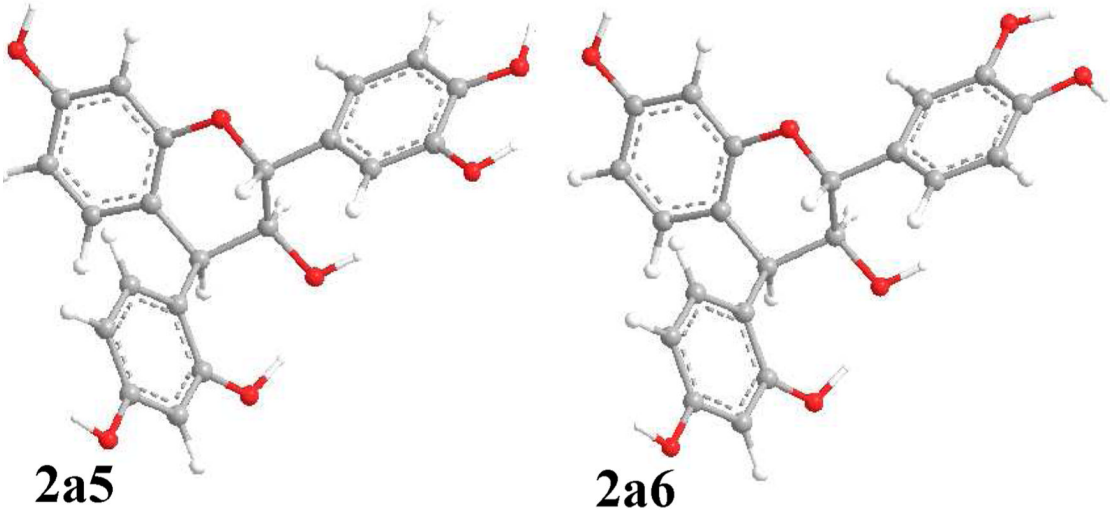

Figure 7.
Potential energy surface and optimized geometries of predominant conformers of compound **2a** at the B3LYP/6–31G* level in the gas phase.

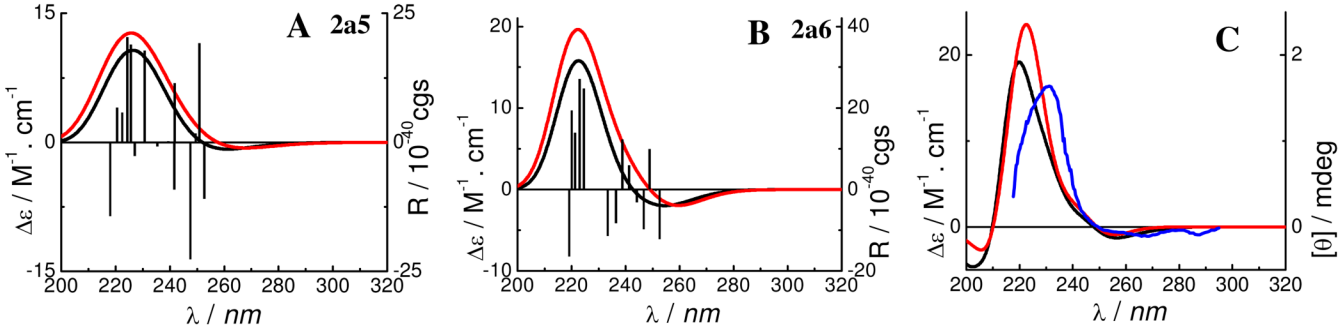

Figure 8.

Calculated and weighted ECD spectra of **2a** and experimental ECD spectrum of **2b**. (—: at the B3LYP/6–31G* level in the gas phase; ▬: at the B3LYP-SCRF/6–31G*//B3LYP/6–31G* level with the COSMO model in MeOH; ▬: the experimental ECD spectrum in MeOH).

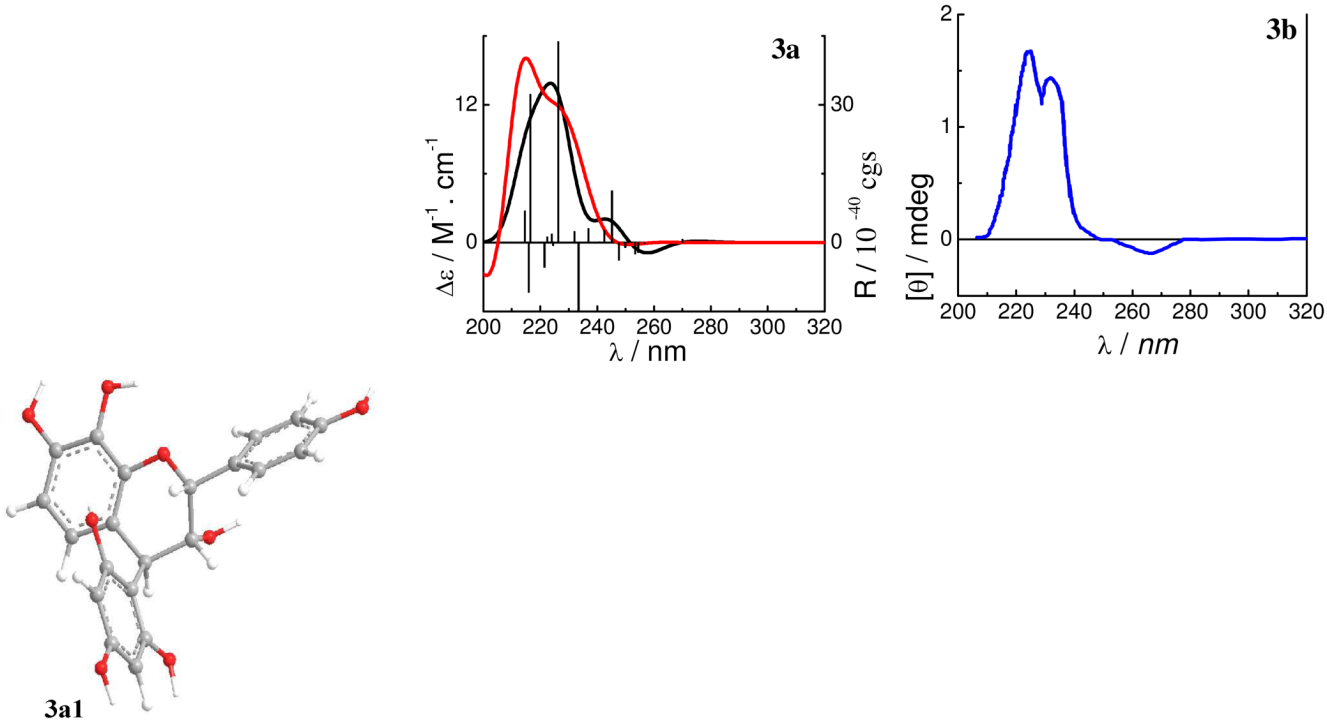

Figure 9.

Optimized geometry of the predominant conformer **3a1** and calculated ECD spectra of compound **3a** and the experimental ECD spectrum of **3b**. (—: at the B3LYP/6–31G* in the gas phase; ▬: at the B3LYP-SCRF/6–31G*//B3LYP/6–31G* level with the COSMO model in MeOH; ▬: the experimental ECD spectrum in MeOH).

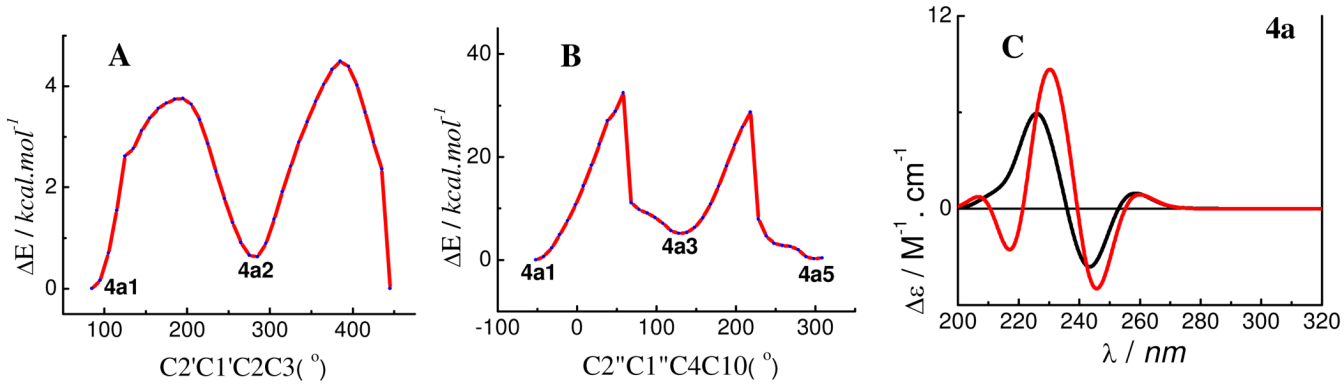

Figure 10.

Potential energy surface of **4a** (A, B) at the B3LYP/6–31G* level and its weighted ECD spectra (C, —: at the B3LYP/6–31G* level in the gas phase; ▬: at the B3LYP-SCRF/6–31G* // B3LYP/6–31G* level).

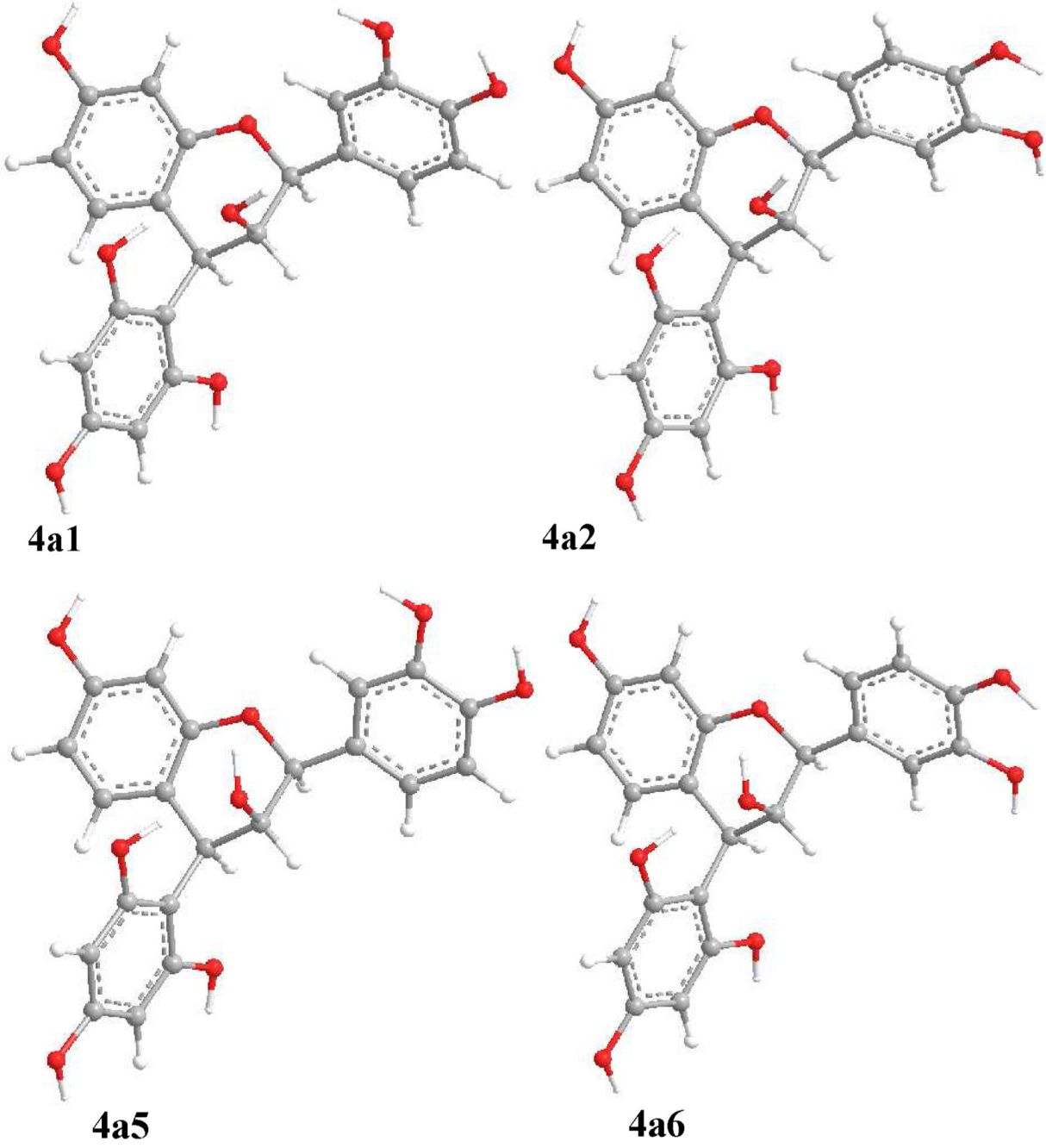

Figure 11.
Optimized geometries of predominant conformers of compound **4a** at the B3LYP/6–31G* level in the gas phase.

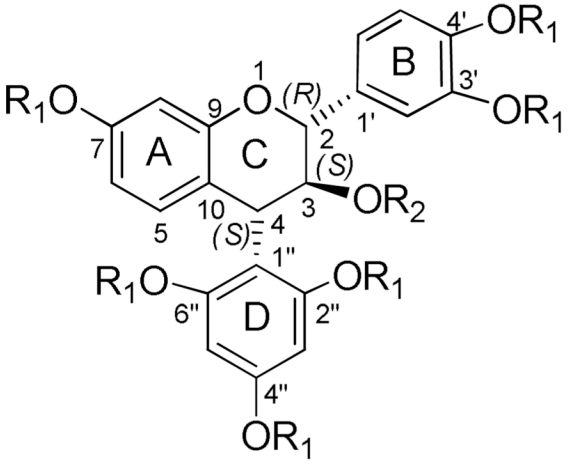

	R_1	R_2
1a	H	H
1b	Me	Ac

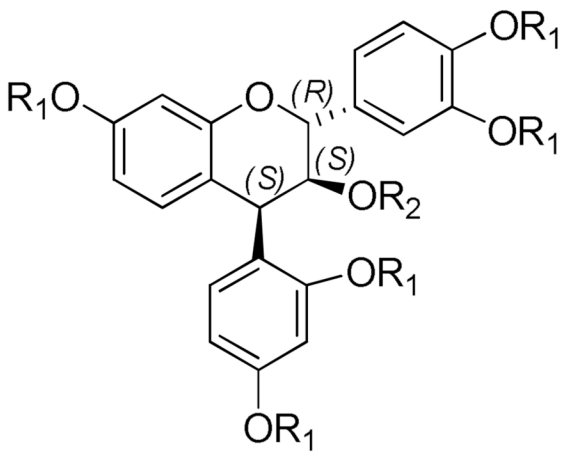

	R_1	R_2
2a	H	H
2b	Me	Ac

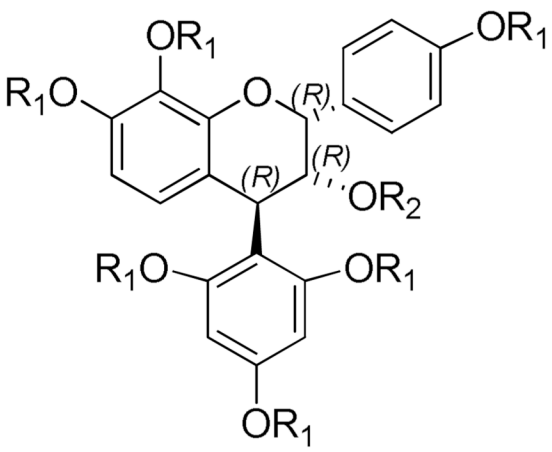

	R_1	R_2
3a	H	H
3b	Me	Ac

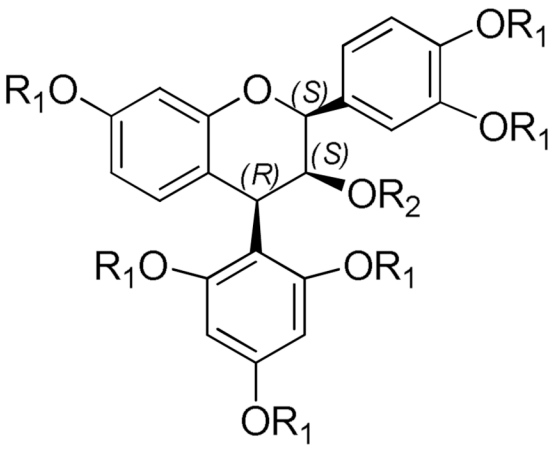

	R_1	R_2
4a	H	H
4b	Me	Ac

Table 1

Conformational Analysis of **1b** in the Gas Phase.

species	ΔE^a	$P_E\%^b$	$\Delta E'^c$	$P_{E'}\%^d$	ΔG^e	$P_G\%^f$
1b1	0.48	20.4	0.49	18.2	0.56	17.3
1b2	0.00	45.8	0.00	41.8	0.00	44.6
1b3	0.67	14.8	0.54	16.9	0.50	19.1
1b4	0.52	19.0	0.35	23.1	0.50	19.0

[a,c,e] Relative energy, relative energy with *ZPE*, and relative Gibbs free energy at the B3LYP/6–31G* level, respectively (kcal/mol).

[b,d,f] Conformational distribution calculated by using the respective parameters above at the B3LYP/6–31G* level.

Table 2

Important Dihedral Angles (°) of Optimized Predominant Conformers at the B3LYP/6–31G* Level in the Gas Phase.

	1a1	1a2	1b1	1b2	1b3	1b4	2a5	2a6	3a1	4a1	4a2	4a5	4a6
H-C2-C3-H	179	179	173	177	178	177	173	173	−62	61	61	71	72
H-C3-C4-H	161	161	166	167	167	168	52	51	−82	−54	−54	−57	−58
C2′-C1′-C2-O1	154	−34	142	−46	146	−45	152	−34	146	−153	31	−169	14
C1′-C2-O1-C9	180	178	174	175	174	174	163	163	167	−164	−164	−175	−176
C2-O1-C9-C10	−26	−26	−20	−20	−20	−20	−9	−9	−12	13	13	20	21
C3-C4-C10-C9	−7	−6	−15	−14	−15	−16	−24	−24	−14	22	22	21	21
C1″-C4-C10-C9	−136	−136	−142	−142	−143	−143	104	104	114	153	153	152	153
C2″-C1″-C4-C10	−142	−142	−118	−118	−118	−117	157	157	−34	−53	−53	−57	−58

Table 3

Conformational Analysis of Compound **1a** (au)

Species	in gas phase								in MeOH	
	ΔE^a	$P_E\%^b$	$\Delta E'^c$	$P_{E'}\%^d$	ΔG^e	$P_G\%^f$	$\Delta E''^g$	$P_{E''}\%^h$	$\Delta E_s{}^i$	$P_{Es}\%^j$
1a1	0.00	57.0	0.00	55.2	0.00	51.9	0.00	50.7	0.18	40.5
1a2	0.17	43.0	0.12	44.8	0.05	48.0	0.02	49.3	0.00	55.2
1a3	5.74	0.0	5.05	0.0	4.17	0.0	4.91	0.0	1.94	2.1
1a4	5.78	0.0	5.00	0.0	3.67	0.1	4.80	0.0	1.90	2.2
1a5	10.81	0.0	10.23	0.0	9.59	0.0		0.0	8.68	
1a6	10.55	0.0	10.09	0.0	9.93	0.0		0.0	8.75	

*a,c,e,g*Relative energy, relative energy with *ZPE*, and relative Gibbs free energy at the B3LYP/6–31G* level, and relative energy at the B3LYP/6–311++G**//B3LYP/6–31G* level, respectively (kcal/mol).

*b,d,f,h*Conformational distribution calculated by using the respective.

*i,j*Relative energy and conformational distribution calculated at the B3LYP-SCRF/6–31G*//B3LYP/6–31g* level with the COSMO model, respectively.

Table 4

Important Transition States, Related Rotatory Strengths, and Oscillator Strengths of **1a1** and **1a2** at the B3LYP/6−31G* Level in the Gas Phase.

species	transition	ΔE^a (eV)	λ^b (nm)	f^c	$R^{vel d}$	$R^{len e}$
1a1	104→105	4.75	261	0.010	−1.6	−1.5
	104→106	4.90	253	0.064	5.3	4.7
	103→105	4.97	250	0.034	−5.7	−3.8
	104→106	5.06	245	0.051	6.5	7.6
	103→105	5.10	243	0.003	5.5	5.3
	102→105	5.14	241	0.001	3.3	3.2
	103→106	5.22	237	0.011	−7.4	−7.2
	104→108	5.45	227.3	0.098	−26.4	−25.9
	102→107	5.46	226.9	0.040	−13.5	−13.0
	100→106	5.59	222	0.039	19.1	18.5
	104→110	5.62	221	0.008	−9.4	−9.8
	100→106	5.64	220	0.010	−15.6	−16.1
	103→109	5.66	219	0.004	16.8	16.2
	101→107	5.74	216	0.015	−20.1	−20.8
1a2	104→105	4.74	261	0.013	10.9	10.6
	104→106	4.90	253	0.042	−20.8	−18.9
	103→105	4.98	249	0.029	21.1	20.0
	102→105	5.02	247	0.006	−5.1	−4.9
	104→106	5.04	246	0.051	12.9	13.8
	103→105	5.08	244	0.006	−4.0	−3.8
	102→105	5.16	240	0.003	4.7	4.4
	103→106	5.23	237	0.018	−9.3	−9.2
	104→108	5.44	228	0.128	−57.2	−56.4
	100→106	5.56	223	0.018	−20.1	−20.4
	104→110	5.63	220.4	0.018	−14.2	−14.7
	100→106	5.65	219.6	0.035	20.1	21.2
	103→109	5.65	219.3	0.013	7.3	6.6

species	transition	ΔE^a (eV)	λ^b (nm)	f^c	$R^{vel d}$	$R^{len e}$
	101→107	5.75	216	0.014	10.9	10.8

[a] Excited energy.

[b] Wavelength.

[c] Oscillator strength.

[d] Rotatory strength in velocity form (10^{-40} cgs).

[e] Rotatory strength in length form (10^{-40}cgs).